Available online at www.sciencedirect.com
SCIENCE DIRECT
Journal of Colloid and Interface Science 284 (2005) 742–752
JOURNAL OF Colloid and Interface Science
www.elsevier.com/locate/jcis

Shear-modulated electroosmotic flow on a patterned charged surface

Hsien-Hung Wei

Department of Chemical Engineering, National Cheng Kung University, Tainan 701, Taiwan

Received 8 June 2004; accepted 19 October 2004

Available online 15 January 2005

Abstract

The effect of imposing shear flow on a charge-modulated electroosmotic flow is theoretically investigated. The flow structures exhibit either saddle points or closed streamlines, depending on the relative strength of an imposed shear to the applied electric field. The formation of closed streamlines could be advantageous for trapping nondiffusive particles at desired locations. Different time periodic alternating flows and their corresponding particle trajectories are also examined to assess strategies for creating efficient mixing.

Keywords: Patterned electroosmotic flow; Shear flow

1. Introduction

Electroosmotic flow (EOF) is an electrokinetic phenomenon in which an electrolyte fluid moves with respect to a stationary charged surface in response to an electric field. An immobile charged surface attracts a cloud of opposite charges, creating a thin electrical double layer (EDL) as a mobile "sheath" of charges next to it. Application of an external electric field results in the movement of this mobile sheath near the surface. The induced momentum is then transmitted to adjacent layers of fluid through the effect of viscosity, as if the walls of the channel were sliding. This creates an EOF.

EOF has recently received much attention because of its potential applications to microfluidics. It not only provides an alternative to pressure-driven flow in microchannels, but also emerges as a potential means to handle a variety of fluids, e.g., separation and mixing. Among recent research developments in EOF, EOF induced by patterned, nonuniform surface charge in particular offers a new paradigm for designing microfluidic devices. Ajdari [1] first demonstrated this idea and showed that spatial modulation of the surface charge density can generate convective rolls induced by EOF. The morphology of these rolls depends on the ratio of the fluid layer thickness to the wavelength of the modulation and on the phase difference of modulated surface charges between the top and bottom surfaces. He further showed that the channel geometry having biased symmetry could also generate a net EOF current, which could be useful in designing micropumps. The strategy for developing an EOF pump by using asymmetric electrode arrays subject to an AC electric field can also be found in his subsequent work [2].

Stroock et al. [3] experimentally investigated EOF with a series of charge-patterned strips and verified recirculating cellular flow patterns. Their measurements of flows agreed well with theory in the limit of thin EDL and low surface potential. As such, the concept of patterned EOF proposed by Ajdari can indeed be realized and justified. Their work also suggested that the induced stagnation-point flow might be used to manipulate macromolecules. Panwar and Kumar [4] adopted this idea to study stretching or trapping of polymer molecules using a patterned EOF.

Qian and Bau [5] used patterned EOF to assess the feasibility of micromixers. They demonstrated that asynchronized time-periodic alternations of the ζ potentials on the top and bottom channel walls could induce chaotic mixing of nondiffusive particles even though there is no net time-averaged flow. This chaotic advection can provide an efficient way to stir fluids in microfluidic devices. The idea to create chaotic advection can be found in the work of

E-mail address: hhwei@mail.ncku.edu.tw.

0021-9797/$ – see front matter
doi:10.1016/j.jcis.2004.10.015

Aref [6]. It essentially involve saddle-point/torus flow structures and the dynamic distortion of these structures [7].

Microfluidic handling often involves various actuation mechanisms, depending on applications. On some occasions, a combination of different actuation means might be required to properly manage flows. For example, superimposing a pressure-driven flow on an EOF may be necessary for electrophoretic separation in view of the resolution of analytes in inhomogeneous zones of electrical conductivity [8]. For another scenario that might occur in a pressure-driven flow, applying a charge-modulated EOF to the preexisting background flow could provide selective fluidic manipulations, e.g., trapping particles in selected regions or separating desired particles from mixture, via judicious control of relative flow strengths. This might provide an additional advantage to particle manipulation. Furthermore, from the viewpoint of generating effective mixing using chaotic motions, imposing an additional external flow on a simple, regularly patterned EOF could result in more intricate flow structures due to complex flow interactions. This not only reduces the needs in more sophisticated fabrication of patterning microchannels for achieving similar effects, but also provides a new route to fluidic handling. As such, a single device combining both patterned EOF and another external flow seems rather appealing to fulfill a variety of purposes of microfluidic usage.

As motivated by the above, we would like to explore how a charge-modulated EOF interacts with a flow driven by another external force. In this article, we consider the simplest system that consists of a patterned EOF and a simple shear flow. This simple system could at least serve as a local flow model for understanding the hydrodynamics in the proximity of the walls of a patterned EOF in the presence of pressure forces.

2. Electroosmosis and hydrodynamics

Consider a flat surface defined at $y = 0$ in the Cartesian coordinates (x, y) depicted in Fig. 1. The electrolyte is an incompressible fluid of dielectric constant ε and viscosity μ, and its ionic content has a Debye–Hückel length of κ^{-1}. The surface acquires charges in contact with the electrolyte, and bears a surface charge density σ. The length scale L over which σ modulates is assumed to be sufficiently longer than the Debye length κ^{-1}. The local electric potential in the fluid-surface vicinity (Debye layer) admits $\phi = \zeta \exp(-\kappa y)$ with the surface potential (or ζ potential) $\zeta = \sigma/\varepsilon\kappa$ due to an excess of opposite charges adjacent to the surface. This applies when the Debye–Hückel approximation is valid for low electrostatic potentials $e\zeta/k_BT \ll 1$.

As an external electric field E is applied parallel to the surface, it drives the fluid within the Debye layer, inducing motions of the bulk fluid parallel to the surface. Let $\mathbf{v} = (u, v)$ denote the velocity field where u and v are the velocity components in the x and y directions, respectively.

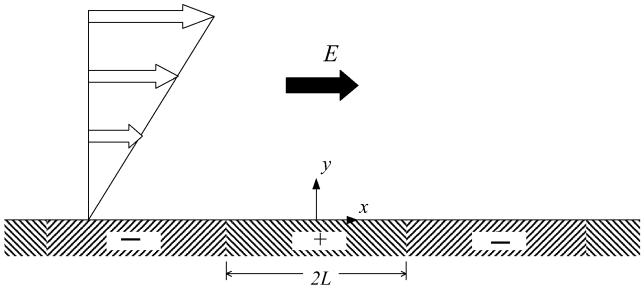

Fig. 1. A charge-modulated electroosmotic flow (EOF) in the presence of a shear flow.

p is the fluid pressure. If the Debye layer is very thin compared with both L and the typical distance of the charge density variation (more precisely, smaller than these lengths by at least a factor $\sim \exp(e\zeta/2k_BT)$ [9]), the motions of the bulk fluid apart from this layer are governed by the Stokes equations:

$$0 = -\nabla p + \mu\nabla^2\mathbf{v}, \tag{1a}$$

$$\nabla \cdot \mathbf{v} = 0. \tag{1b}$$

The system is subject to the slip boundary condition on the surface near which the linear Smoluchowski velocity on the edge of the thin Debye layer is applied:

$$u(y = 0) = -\frac{\varepsilon\zeta}{\mu}E. \tag{2}$$

To describe the flow field, it is more convenient to introduce the stream function ψ such that

$$u = \frac{\partial\psi}{\partial y} \quad \text{and} \quad v = -\frac{\partial\psi}{\partial x} \tag{3}$$

automatically satisfy the continuity equation (1b). For a modulated surface charge density $\sigma(x) = \sigma_0\cos(kx)$ ($k = \pi/L$), the flow field of such an EOF is given by

$$\psi_{\text{EOF}} = -\frac{\varepsilon\zeta_0 E}{\mu}y\exp(-ky)\cos(kx), \tag{4a}$$

$$u_{\text{EOF}} = -\frac{\varepsilon\zeta_0 E}{\mu}(1 - ky)\exp(-ky)\cos(kx), \tag{4b}$$

$$v_{\text{EOF}} = -\frac{\varepsilon\zeta_0 E}{\mu}ky\exp(-ky)\sin(kx), \tag{4c}$$

where $\zeta_0 = \sigma_0/\varepsilon\kappa$. This EOF field has been reported by Ajdari [1].

The linearity of Stokes flows allows the superposition of a shear flow on the above EOF. A shear flow is represented by

$$\psi_{\text{Sh}} = \frac{1}{2}\dot{\gamma}y^2, \tag{5a}$$

$$u_{\text{Sh}} = \dot{\gamma}y, \tag{5b}$$

where $\dot{\gamma}$ is the strain rate. The overall flow field combining both (4) and (5) becomes

$$\psi = \psi_{\text{EOF}} + \psi_{\text{Sh}}, \tag{6a}$$

$$u = u_{\mathrm{EOF}} + u_{\mathrm{Sh}}, \tag{6b}$$

$$v = v_{\mathrm{EOF}}. \tag{6c}$$

3. Flow patterns and characterization

We first present a pure charge-modulated EOF described by Eq. (4) as a reference case for the later comparison with those mediated by imposed shear flows. Typical streamlines of a patterned EOF exhibit cellular flow structures as shown in Fig. 2a. Since the $\sigma > 0$ (< 0) surfaces attract negative (positive) charges that drag the bulk fluid to move toward the high (low)-potential regions when undergoing an electric field, the resulting flows are clockwise (counterclockwise) in response to the applied electric field whose direction is from left to right. This also can be easily understood in view of Eqs. (4b) and (4c). The dividing streamlines between adjacent convective rolls are located at $x = \pi(n + \frac{1}{2})/k$ ($n = 0, \pm1, \pm2, \ldots$), the same locations distinguishing $\sigma > 0$ and $\sigma < 0$ regions, i.e., the roots of $\cos(kx) = 0$. These features have been demonstrated by Ajdari [1].

When an additional shear is exerted on the above EOF, the flow structures depend on a dimensionless parameter $\Gamma \equiv \mu\dot{\gamma}L/\varepsilon\zeta_0 E$, the relative strength of an imposed shear to the applied electric field. Figs. 2b–2d show streamline patterns for various nonzero Γ. For $\Gamma = 0.01$ (Fig. 2b), even though the strength of shear flow is only 1% of EOF, the streamlines exhibit saddle points in the vicinity of free streams and convective EOF rolls. These saddle points form just above counterclockwise EOF rolls whose circulating di-

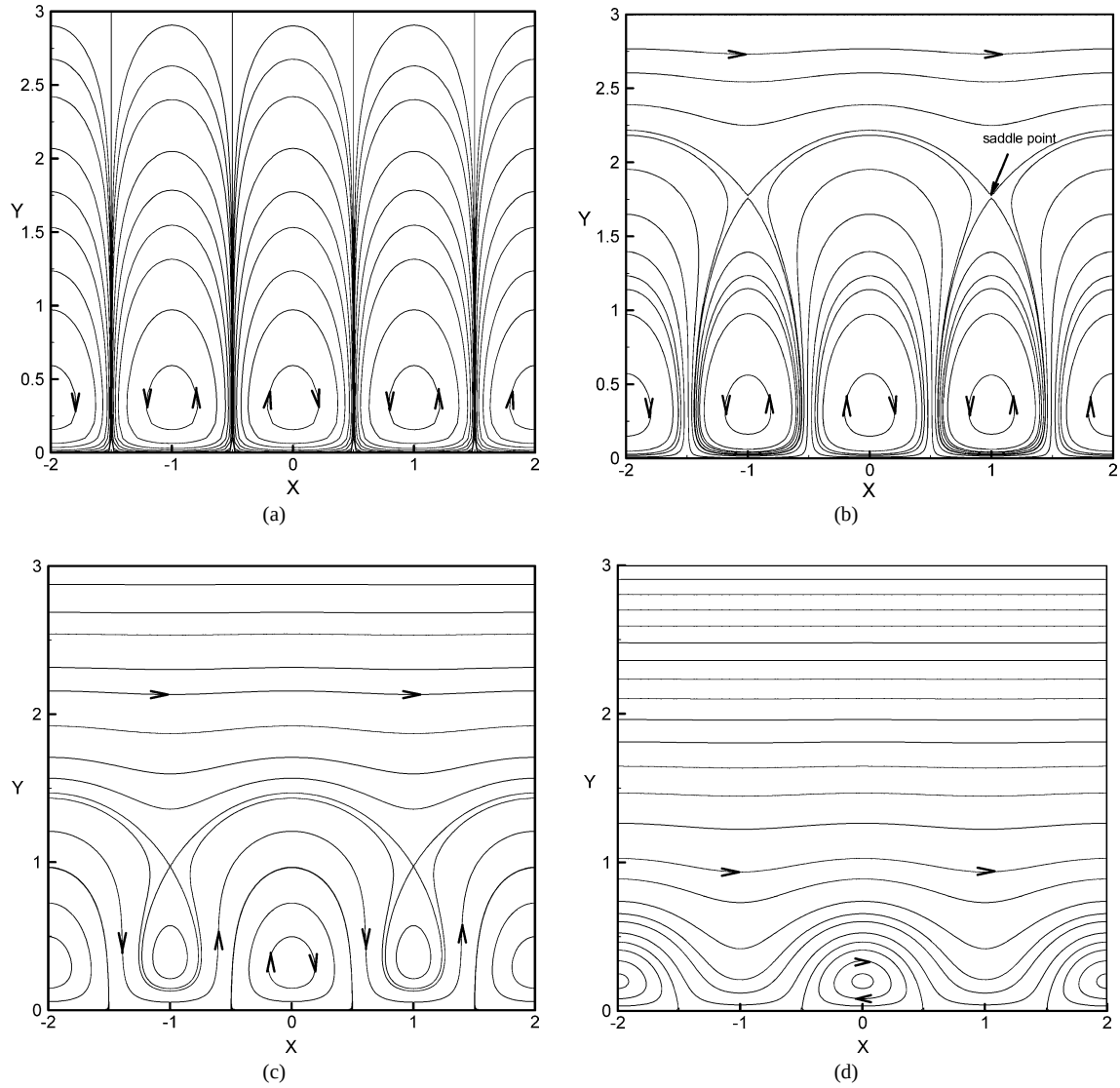

Fig. 2. Streamline patterns for various Γ (the relative flow strength of an imposed shear to EOF). (a) $\Gamma = 0.0$. In the absence of shear flow, a pure charge-modulated EOF in response to an applied electric field E (from left to right) exhibits convective rolls whose flow directions are counterclockwise (clockwise) for the surface charge density $\sigma > 0$ (< 0). (b) $\Gamma = 0.01$. Applying a minute shear causes saddle points in the regions of $\sigma < 0$. Closed streamlines are formed in the regions of $\sigma > 0$. (c) $\Gamma = 0.1$. The EOF rolls are further suppressed by the shear flow as Γ increases. (d) $\Gamma = 1.0$. The counterclockwise EOF rolls for $\sigma < 0$ are now completely suppressed by the shear flow. The clockwise EOF rolls for $\sigma > 0$ are confined by closed streamlines.

rections defy that of the shear flow. Moreover, additional streamlines enclosing clockwise EOF rolls also form because their circulations comply with the shear flow.

As Γ increases to 0.1 as in Fig. 2c, saddle points move toward the wall and the roll structures become smaller than those of Fig. 2b. This is expected because the stronger the shear flow, the more suppression EOF rolls undergo. For $\Gamma = 1$ (Fig. 2d), counterclockwise rolls are completely suppressed by the shear flow, and saddle points no longer appear. Clockwise rolls are still present, but are now confined within even smaller regions. For large Γ, the fluid motion is dominated by a shear flow and EOF-induced rolls eventually vanish as $\Gamma \to \infty$.

Inspecting how the locations of saddle points or stagnation points change with Γ provides more insights into how the flow patterns alter. The saddle/stagnation points admit zero velocities within the flow domain. Scrutinizing Eq. (6) reveals that the y-component velocity Eq. (6c) $v = 0$ demands

$$\sin(kx) = 0 \quad \text{or} \quad kx = n\pi. \tag{7a}$$

This specifies the locations of stationary points in the x direction. It also manifests that these x locations are independent of Γ. Substituting Eq. (7a) into the x-component Eq. (6b) yields the following equation that determines the y positions of these stationary points:

$$\Gamma Y = (-1)^n (1 - \pi Y) \exp(-\pi Y). \tag{7b}$$

Here, $Y = y/L$. For a given Γ, Eqs. (7a) and (7b) determine the locations of saddle/stagnation points. We also find that for an even n, it admits only one solution for Y, while the odd-n case has two solutions. The observations from Fig. 2 suggest that the even-n case associates with the centers of clockwise rolls; the odd-n case corresponds to either saddle points or the centers of counterclockwise rolls. Let us take $\Gamma = 0.01$ as an example for illustrating the occurrences of these points. For $0 \leqslant x \leqslant L$, $n = 0$ yields $(x, y) \approx (0, 0.316L)$, whereas $n = 1$ results in $(x, y) \approx (L, 0.321L)$ or $(L, 1.767L)$. These are confirmed by the observations in Fig. 2a. We also verify the cases for other values of Γ and their results indeed agree with those predicted by Eqs. (7a) and (7b). Further note that $\Gamma = 0$ admits only the stagnation points at $(x, y) = ((n + \frac{1}{2})L, L/\pi)$.

Fig. 2 suggests that there is a critical Γ, Γ^*, beyond which counterclockwise rolls are completely suppressed by a shear flow. Inspecting Eq. (7b) reveals that for odd n, the roots can be determined by the interception between the straight line ΓY and the curve $(\pi Y - 1)\exp(-\pi Y)$. Varying Γ until the former is tangential to the latter can determine Γ^*. This occurs when

$$\Gamma = \pi(2 - \pi Y)\exp(-\pi Y). \tag{8}$$

Together with Eq. (7b), one can analytically obtain $Y = Y^* \equiv (1 + \sqrt{5})/2\pi \approx 0.515$ and $\Gamma^* = \pi(2 - \pi Y^*)e^{-\pi Y^*} \approx 0.238$. This can also be verified by observing the changes in stream patterns for different Γ.

In the limits of both small and large Γ, it is straightforward to obtain the y locations of the corresponding stationary points using Eq. (7b). In the limit of $\Gamma \to 0$, there are two solutions for Y. One solution is $Y \to 1/\pi \sim 0.318$, which is just the y location of the center of any EOF convective roll as depicted in Fig. 2a. Another is $Y \to \infty$ obtained from Eq. (7b) in a form divided by Γ. This can be regarded as the situation where saddle points occur at infinity as $\Gamma \to 0$ indicated by Fig. 2a. As $\Gamma \to \infty$, it leads to $Y \to 0$ as expected for a sufficiently strong shear flow. Figs. 3a and 3b show the dependence of Y on Γ for clockwise roll (even n) and counterclockwise roll (odd n) regions, respectively. As shown in Fig. 3a for a clockwise roll region that admits only one stationary point (i.e., the center of cir-

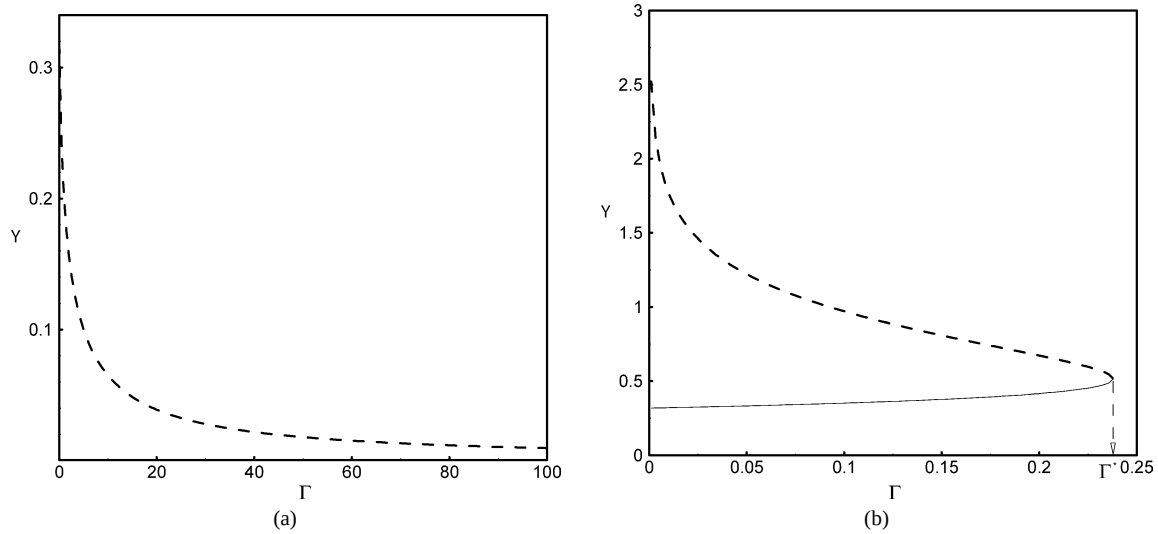

Fig. 3. Vertical locations of stagnation points for (a) $\sigma > 0$ and (b) $\sigma < 0$ regions. Case (a) admits only a single stagnation point that corresponds to the center of a clockwise roll. Case (b) has two stagnation points: the saddle point (dashed line) and the center of a counterclockwise roll (solid line). Both lines merge at $\Gamma = \Gamma^*$ beyond which EOF rolls are completely suppressed by a shear flow.

culation), Y rapidly decreases from $1/\pi$ ($\Gamma \to 0$ limit) to 0 ($\Gamma \to \infty$ limit) as Γ increases, which is expected. On the other hand, for a counterclockwise roll region as in Fig. 3b, the locations of two stationary points behave differently in response to Γ. The higher one corresponds to a saddle point. It falls from ∞ ($\Gamma \to 0$ limit) as Γ increases. The lower one associates with the center of a recirculation and slightly rises from $1/\pi$ ($\Gamma \to 0$ limit) as Γ increases. Two points merge at $\Gamma = \Gamma^*$, beyond which counterclockwise rolls are completely suppressed by the shear flow.

The effect of shear flow on flow structures can also be understood in conjunction with the closed streamlines that confine counterclockwise EOF rolls. These streamlines have $\psi = 0$ within the flow domain and can be found according to (6a):

$$\frac{1}{2}\Gamma Y \exp(\pi Y) = \cos(\pi X), \tag{9}$$

where $X = x/L$. Equation (9) indicates that the closed streamlines occur only for $\cos(\pi X) > 0$ or the $\sigma > 0$ surfaces. As $\Gamma \to 0$, Eq. (9) immediately yields $\cos(\pi X) = 0$ or $X = n + \frac{1}{2}$. This signifies that the $\Gamma \to 0$ streamlines for confining EOF rolls can be thought of as "closing at infinity" or becoming vertical, as shown in Fig. 2a. As $\Gamma \to \infty$, Eq. (9) leads to $Y \to 0$ for arbitrary X, which is just the wall.

4. Particle trajectories and mixing

With the velocity field [(6b) and (6c)], the motion of a passive (nondiffusive) tracer particle can be determined by the following kinematic equations:

$$\frac{\partial x}{\partial t} = u, \tag{10a}$$

$$\frac{\partial y}{\partial t} = v. \tag{10b}$$

For a steady flow, particles just follow streamlines and there is clearly no mixing. To create effective mixing, one can temporally modulate EOF, shear flow, or their combination. The temporal modulation of EOF can be used by time-periodic ζ potentials via application of alternative current to embedded electrodes. As long as the time required to reach the electrostatic equilibrium and the viscous time scale are much shorter than the oscillation period, the flow field can be regarded as a quasi-steady Stokes flow described by Eqs. (6).

We first consider an EOF with a time-oscillatory ζ potential $\zeta = \zeta_0 f(\omega t)$, where f is a time-modulating function with frequency ω. We can rewrite Eqs. (10a) and (10b) in the following dimensionless form:

$$\mathrm{St}\frac{\partial X}{\partial \tau} = \Gamma Y - f(\tau)(1 - \pi Y)\exp(-\pi Y)\cos(\pi X), \tag{11a}$$

$$\mathrm{St}\frac{\partial Y}{\partial \tau} = -f(\tau)\pi Y \exp(-\pi Y)\sin(\pi X), \tag{11b}$$

where the dimensionless time is $\tau = \omega t$ and the Stokes number $\mathrm{St} = \mu L\omega/(\varepsilon\zeta_0 E)$ is defined as the time-scale ratio of EOF to temporal oscillation. To ensure the validity of quasi-steady Stokes flows for the present analysis, a sufficiently long oscillation time scale compared with the viscous time scale demands $\rho\omega L^2/\mu \ll 1$ (ρ is the fluid density). For $\rho = 1$ g/cm^3, $\mu = 0.01$ P, and $L = 100$ μm as in typical microfluidic applications, the frequency ω is required $\ll 10^2$. This frequency constraint thus prevents the occurrences of high-frequency (> 1 kHz) electrokinetic phenomena such as dielectrophoresis [10] and surface polarization [2].

It might be instructive to first observe the temporal stream patterns for Eqs. (11) prior to understanding the corresponding particle trajectories. For $\Gamma = 0.01$ and $f(\tau) = \sin(\tau)$, Fig. 4 shows some snapshots of the stream patterns dur-

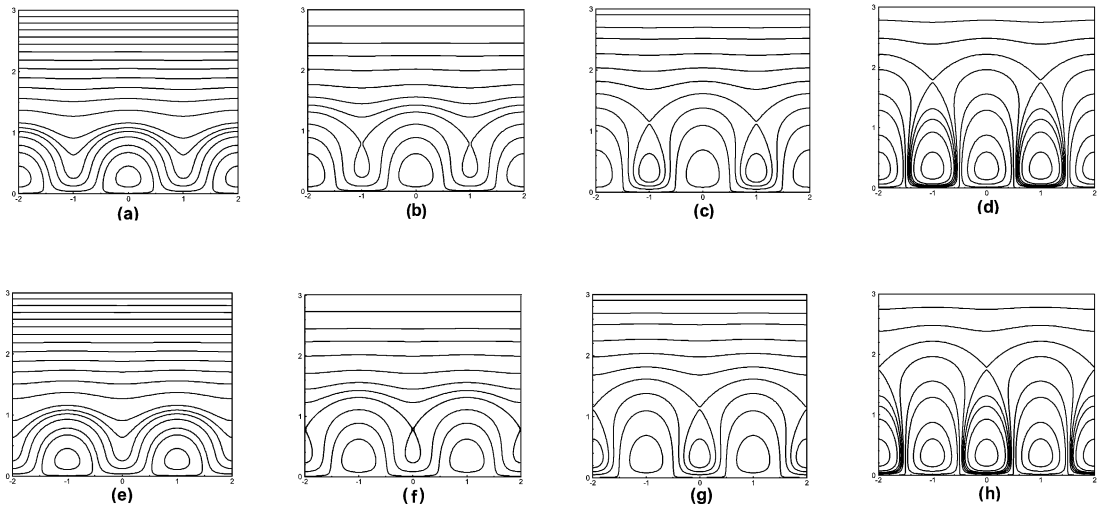

Fig. 4. Some snapshots of the streamlines during a cycle for a system consisting of a time-periodic EOF and a steady shear flow. $\Gamma = 0.01$. (a) $\tau = 0.01\pi$, (b) $\tau = 0.02\pi$, (c) $\tau = 0.05\pi$, (d) $\tau = 0.5\pi$, (e) $\tau = 1.01\pi$, (f) $\tau = 1.02\pi$, (g) $\tau = 1.05\pi$, (h) $\tau = 1.5\pi$. For $\tau = 0$–0.5π, the strength of EOF gradually increases and EOF rolls and thus expands. For $\tau = 0.5\pi$–π, the flow acts in the reverse sequence of those during $\tau = 0$–0.5π. For $\tau = \pi$–1.5π, the surface charges change the signs and the resulting EOF rolls alter accordingly. The stream patterns during $\tau = 1.5\pi$–2π are in the reverse sequence of those during $\tau = \pi$–1.5π.

ing an oscillation cycle. At the earlier stages of the cycle ($\tau = 0.01\pi$, Fig. 4a), the strength of EOF is weak, and only clockwise circulations form above the $\sigma > 0$ surfaces. As EOF gradually becomes strong at later times ($\tau = 0.02\pi$–0.05π, Figs. 4b and 4c), additional counterclockwise rolls and saddle points appear above the $\sigma < 0$ surfaces. These structures grow as EOF strength increases. At $\tau = 0.5\pi$, the moment when EOF strength reaches the maximum, the roll structures become the largest (Fig. 4d). During $\tau = 0.5\pi$–π, the process is reversed due to a gradually weakening EOF. In the remainder of the cycle, the surface charge distribution changes alternatively; the surface with $\sigma < 0$ ($\sigma > 0$) in the previous half-cycle now switches to $\sigma < 0$ ($\sigma > 0$). The corresponding stream patterns thus change accordingly. Figs. 4e–4h illustrate the stream patterns during $\tau = \pi$–1.5π. Once again, the stream patterns during $\tau = 1.5\pi$–2π are in the reverse sequence of those during $\tau = \pi$–1.5π.

Fig. 5 shows the particle trajectories with $\mathrm{St} = 1$ for the flow system of Fig. 4. The trajectories display different spatially periodic patterns for various initial positions. The results show that the closer a particle is placed to the wall, the more distortion its trajectory exhibits. Various trajectory patterns can be understood by the fact that different particle positions experience different degrees of shear–EOF interactions. Recall that for a steady flow of $\Gamma = 0.01$, free streams and convective rolls are separated by the dividing streamline past the saddle points $(X, Y) = (n, 1.767)$, where n is an odd integer. When particles are placed within the free-stream region, they are primarily advected by the shear flow and their transverse motions are slightly modulated by the time-periodic EOF. However, those placed close to the recir-

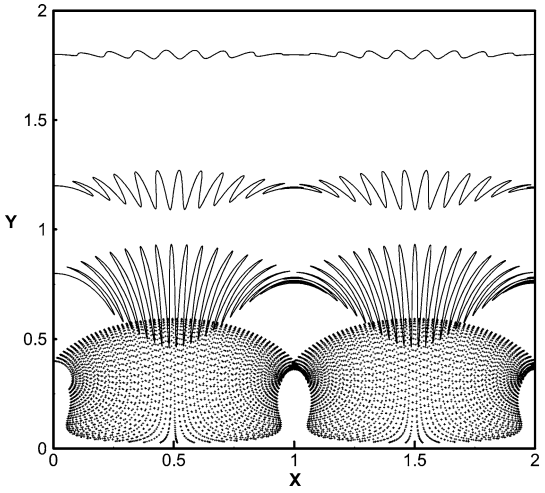

Fig. 5. Particle trajectories of a time-periodic EOF in the presence of a steady shear. $\Gamma = 0.01$, $\mathrm{St} = 1.0$. From top to bottom, curves represent various initial positions, $(X_0, Y_0) = (0.0, 1.8), (0.0, 1.2), (0.0, 0.8), (0.0, 0.4)$.

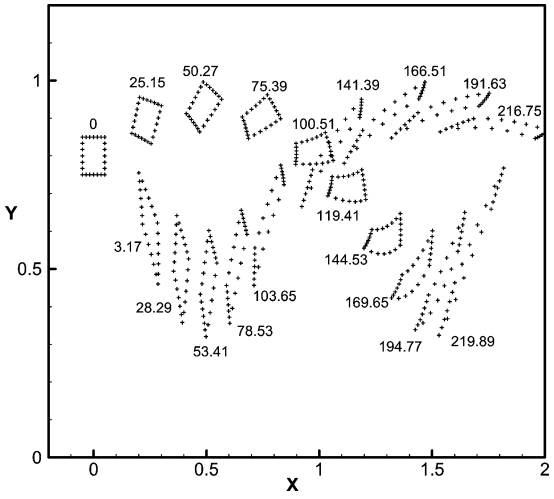

Fig. 6. Spatiotemporal evolution of blob deformation. A square blob of edge size 0.1 is initially centered at $(0.0, 0.8)$. The flow conditions are the same as in Fig. 5. Various numbers associated with different blobs indicate times.

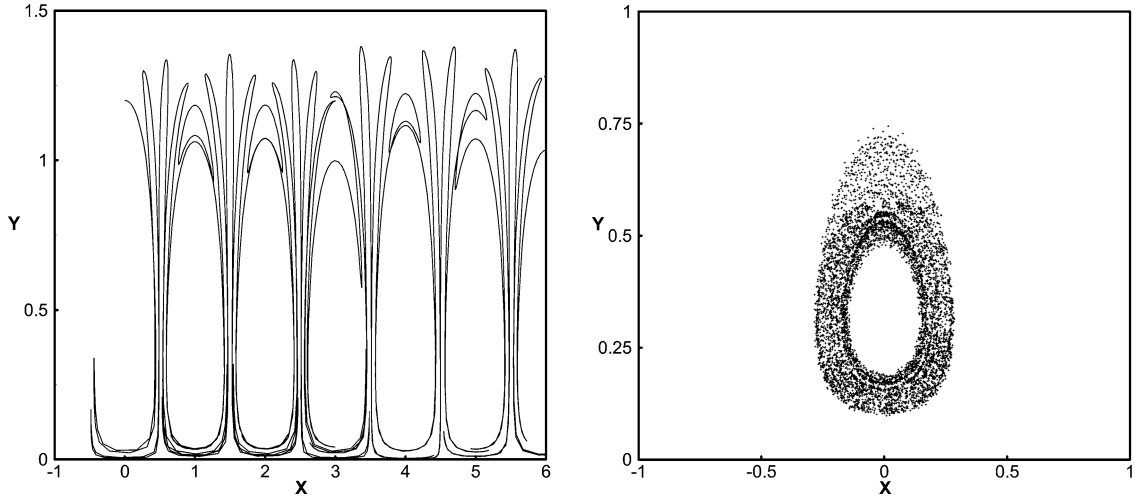

Fig. 7. Particle trajectories of a time-periodic EOF in the presence of a steady shear. $\Gamma = 0.01$, $\mathrm{St} = 0.2$. The initial particle positions are (a) $(X_0, Y_0) = (0.0, 1.2)$ and (b) $(X_0, Y_0) = (0.0, 0.5)$.

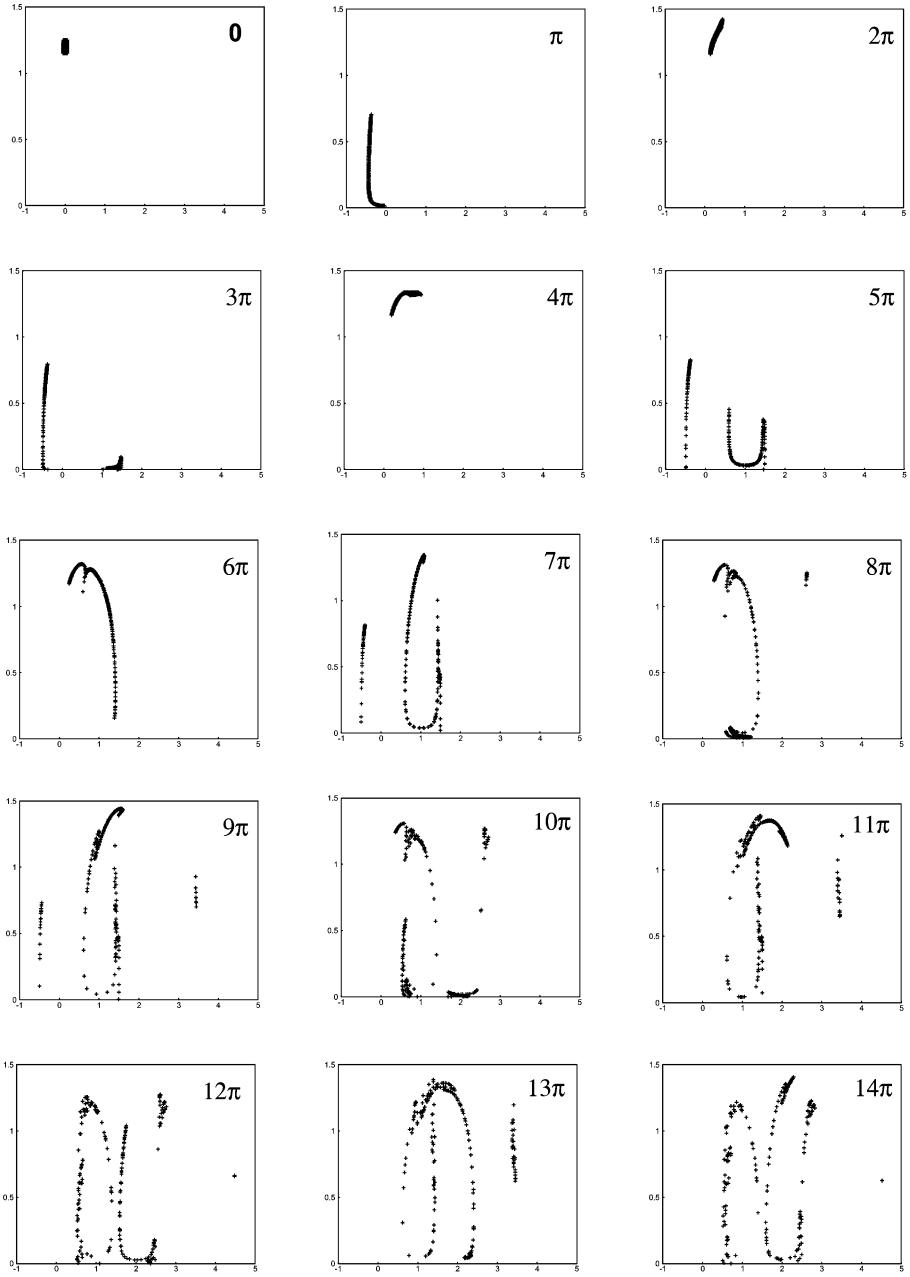

Fig. 8. Spatiotemporal evolution of blob deformation. A square blob of edge size 0.1 is initially centered at (0.0, 1.2). The flow conditions are the same as in Fig. 7. Numbers indicate times.

culation regions are strongly influenced by the alternation of time-periodic EOF patterns (see Fig. 4), thereby leading to zig-zag or stretching/folding of particle motions.

To better describe mixing processes, like Aref [6], we also perform simulations for observing the evolution of a blob of passive tracers in the flow. For the flow system described in Fig. 4, a square material blob with edge size 0.1 is initially centered at (0.0, 0.8), and its spatiotemporal evolution is shown in Fig. 6. The result shows that the blob undergoes deformation/stretching as it advects downstream.

Fig. 7 shows the particle trajectories for $\Gamma = 0.01$ and $\mathrm{St} = 0.2$. In this case, the oscillation period is longer than the EOF time scale. Particles thus have a relatively longer time to interact with a slowly varying EOF. In contrast to the $\mathrm{St} = 1$ case, a particle placed within the free-stream region (Fig. 7a) can penetrate the EOF roll regions near the wall because of the long oscillation time scale. As this particle is continuously advected downstream by the shear flow, it moves in a manner somewhat portraying the EOF roll structures. More interestingly, the spatial structure of the trajectory exhibits a quasi-periodic pattern. For particles placed near the recirculation regions, stretching and folding of fluid elements roughly resemble EOF rolls. These particles could exhibit either dispersive, quasi-periodic trajecto-

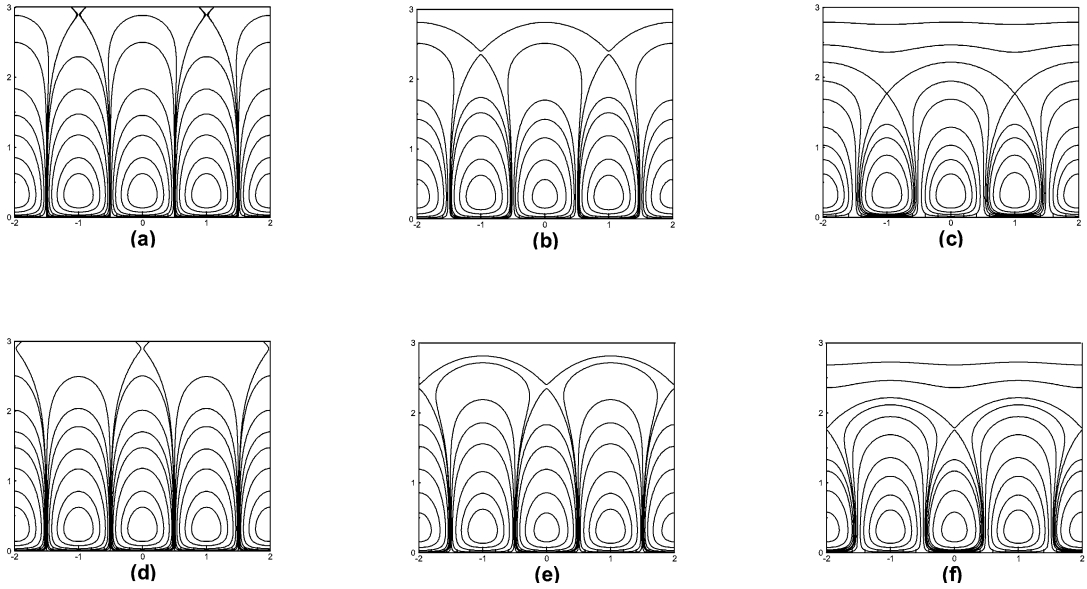

Fig. 9. Some snapshots of the streamlines during a cycle for a steady EOF modulated with a time-periodic shear. $\Gamma = 0.01$. (a) $\tau = 0.01\pi$, (b) $\tau = 0.05\pi$, (c) $\tau = 0.5\pi$, (d) $\tau = 1.01\pi$, (e) $\tau = 1.05\pi$, (f) $\tau = 1.5\pi$. For $\tau = 0$–0.5π, a gradually strong shear suppresses EOF rolls. For $\tau = 0.5\pi$–π, the flow acts in the reverse sequence of those during $\tau = 0$–0.5π. For $\tau = \pi$–1.5π, the direction of the shear is reversed. Saddle points and closed streamlines change accordingly. The stream patterns during $\tau = 1.5\pi$–2π are in the reverse sequence of those during $\tau = \pi$–1.5π.

ries or nondispersive, confined orbits with respect to stagnation points as depicted in Fig. 7b. Fig. 8 shows the evolution of a blob initially centered at (0.0, 1.2) for the flow system of Fig. 7. Stretching/folding of the blob basically portrays the outlines of EOF rolls as trace particles moves downstream, suggesting that the mixing process is dispersive.

The above illustrates the particle trajectories and blob evolution for a time-periodic EOF in the presence of a steady shear flow. We now consider another situation where a steady EOF is modulated with a time-periodic shear flow. The shear flow varies sinusoidally with time according to $g(\tau) = \sin(\tau)$. In this case, the particle trajectories are determined by

$$\mathrm{St}\frac{\partial X}{\partial \tau} = \Gamma g(\tau) Y - (1 - \pi Y)\exp(-\pi Y)\cos(\pi X), \qquad (12a)$$

$$\mathrm{St}\frac{\partial Y}{\partial \tau} = -\pi Y \exp(-\pi Y)\sin(\pi X). \qquad (12b)$$

We again inspect the stream patterns during a cycle and show some snapshots in Fig. 9. At the earlier stages of the cycle (Figs. 9a and 9b), the shear strength is weak and EOF dominates the flow structures. At later times, the shear gradually becomes strong and suppresses EOF. At $\tau = 0.5\pi$ (Fig. 9c), the shear strength reaches a maximum. The shear strength then gradually falls during $\tau = 0.5\pi$–π and the flow patterns are in the reverse sequence of those during $\tau = 0$–0.5π. For $\tau = \pi$–2π, the direction of the shear flow is reversed. The resulting flow structures are similar to those during $\tau = 0$–π. The only difference here is that saddle points occur within clockwise roll regions instead of counterclockwise roll regions during $\tau = 0$–π. Figs. 9d–9f illustrate some stream patterns during $\tau = \pi$–1.5π and those during $\tau = 1.5\pi$–2π can be regarded as in a reverse sequence.

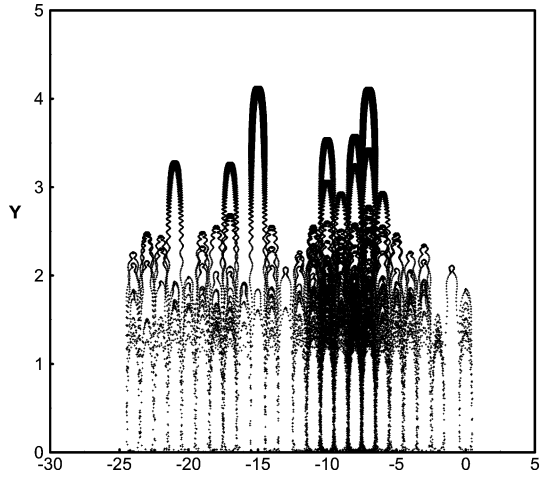

Fig. 10. Particle trajectory for a steady EOF modulated with a time-periodic shear. $\Gamma = 0.01$, $\mathrm{St} = 0.2$. The initial particle position is $(X_0, Y_0) = (0.0, 1.8)$.

Fig. 10 shows the particle trajectory with $\mathrm{St} = 0.2$ for the flow system of Fig. 9. Although the trajectory somewhat resembles cellular flow patterns, it exhibits less regular patterns compared with those of Fig. 7 for the time-periodic EOF case. In addition, particles can be dispersed into much deeper and wider regions as time proceeds. The evolution of a blob (Fig. 11) also exhibits similar features as above.

If both EOF and shear flow alternate periodically with time, but with a phase difference between them, they could induce chaotic advection [6]. For $\Gamma = 1.0$ and $\mathrm{St} = 0.2$, we consider the case in which EOF and shear modulate with $f(\tau) = \cos(\tau)$ and $g(\tau) = \sin(\tau)$, respectively. The particle trajectory is shown in Fig. 12 and exhibits even irregular or

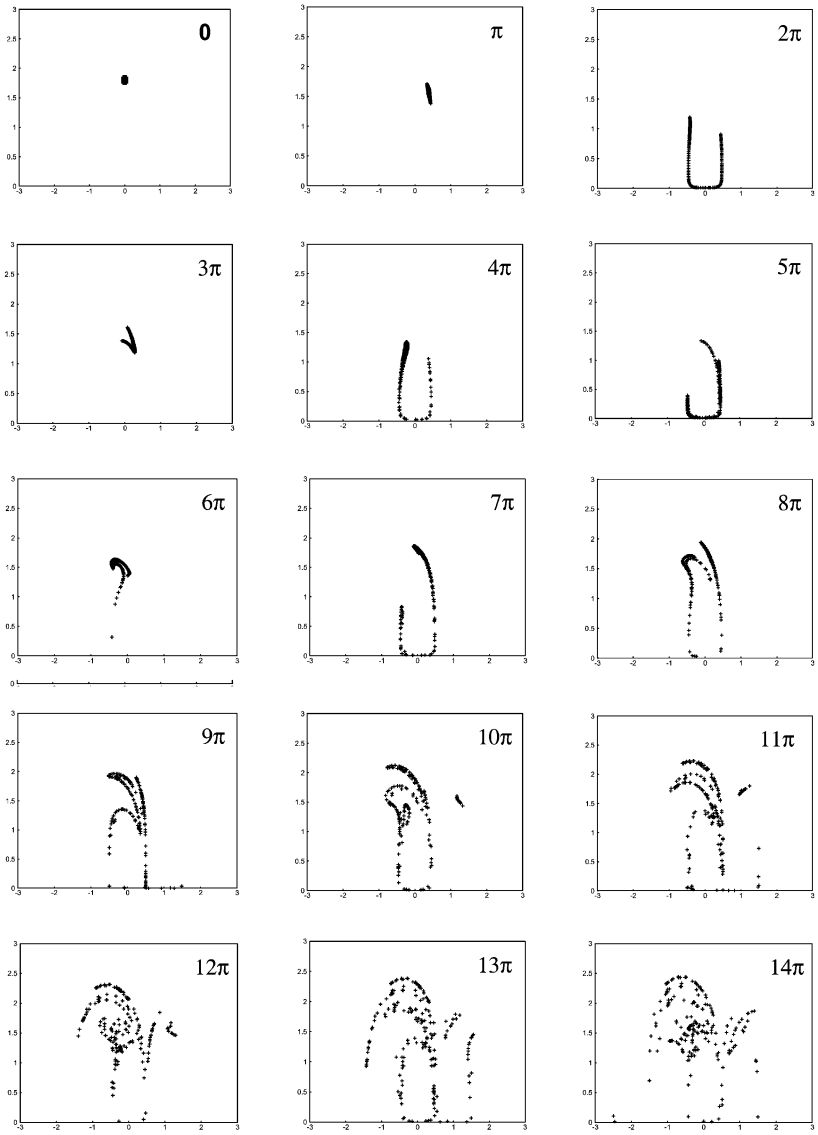

Fig. 11. Spatiotemporal evolution of blob deformation. A square blob of edge size 0.1 is initially centered at (0.0, 1.8). The flow conditions are the same as in Fig. 10. Numbers indicate times.

chaotic patterns compared with Fig. 10. Fig. 13 shows the corresponding blob evolution. In comparison with Fig. 11, since tracers travel with a stronger shear flow, they have larger displacements and move back and forth very rapidly. These tracers gradually disperse toward the wall due to the EOF, while their longitudinal dispersions are relatively weak because of the rapidly changing shear flow.

5. Concluding remarks

We have analytically examined how the presence of a shear flow modulates the flow structure of a patterned EOF. When the shear strength is relatively weak compared with that of EOF, the flow structure can exhibit saddle points. When EOF is weak, its interaction with shear flow could lead to closed streamlines. This is particularly useful in trapping nondiffusive particles within desired locations. For example,

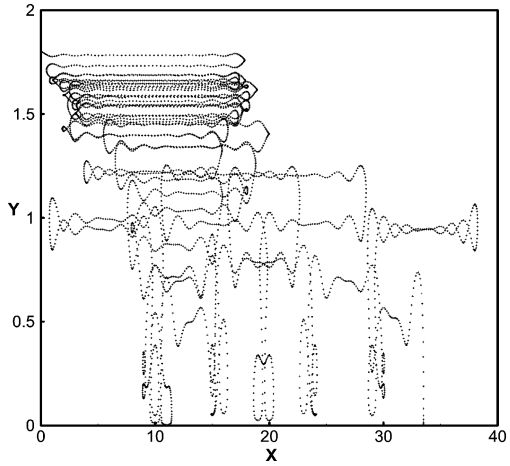

Fig. 12. Particle trajectory of a system subject to both time-alternating EOF and shear flow. The EOF and shear flow modulate with $\cos(\tau)$ and $\sin(\tau)$, respectively. $\Gamma = 1.0$, $\mathrm{St} = 0.2$. The initial particle position is $(X_0, Y_0) = (0.0, 1.8)$. The trajectory is less regular compared with Fig. 10.

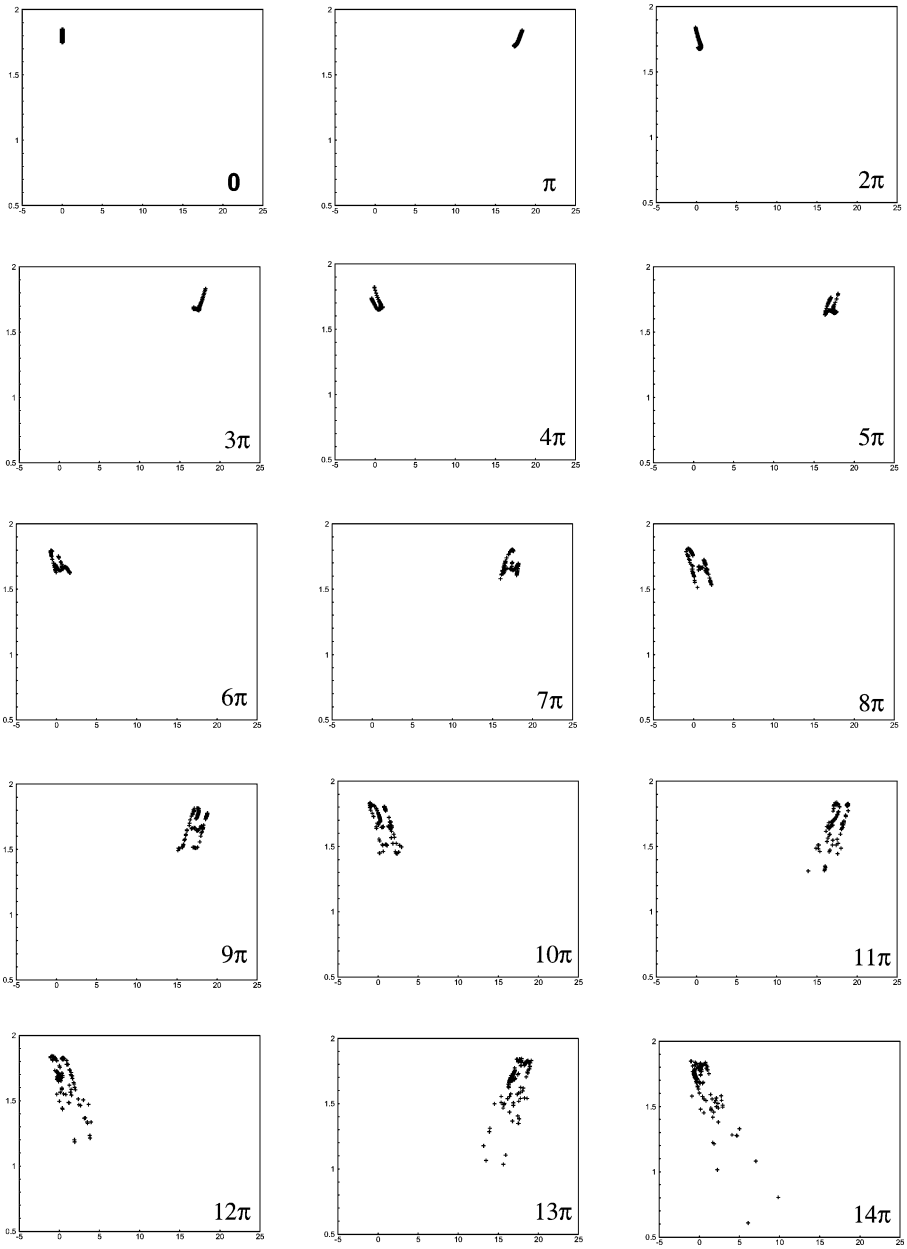

Fig. 13. Spatiotemporal evolution of blob deformation. A square blob of edge size 0.1 is initially centered at (0.0, 1.8). The flow conditions are the same as in Fig. 12. Numbers indicate times.

consider a pressure-driven flow in a microchannel. One can arrange embedded electrodes for generating patterned surface charges within a certain region of the channel. In the absence of an electric field, particles simply advect with a parallel flow. These particles could travel at different positions across the channel according to differences in their physical properties (e.g., size, density). When targeted particles arrive at desired locations, activating a patterned EOF for forming closed streamlines can trap these particles therein; those outside the closed-streamline regions just keep traveling downstream. After depletion of nontargeted particles, previously trapped particles can be released by deactivating the electric field. They can then be redirected for other handling or detection. As such, the separation of particles can be realized by the above processes.

We further explore the potential usage to create effective mixing via temporal modulation between shear flow and patterned EOF. Temporal alternation of EOF results in quasi-periodic particle motions. A steady patterned EOF modulated with a time-periodic shear flow can exhibit less regular patterns of particle trajectories. When both patterned EOF and shear flow alternate with time, this flow system could induce chaotic advection. The behaviors of mixing for different time-alternating shear–EOF systems are also characterized by the evolutions of square blobs. These results suggest that proper control of time-alternating schemes might

provide a means to achieve efficient stirring in microfluidic systems without using any moving parts.

The present work focused on how a patterned EOF interacts with an imposed shear. This can be regarded as modeling local flow behaviors near the wall for a pressure-driven channel flow accompanying a patterned EOF. The extension of our current study to channel systems is straightforward. As already shown in the study of Ajdari [1], EOF convective rolls exhibit various patterns, depending on the height of the channel and the arrangement of surface charge modulation on the top and bottom surfaces. Qian and Bau [5] adopted this idea to create chaotic advection via timewise alternations of the ζ potentials. When these EOFs undergo additional pressure forces, the flow interactions could lead to more complicated flow structures. For a sufficiently strong pressure force or a large channel gap, the flow features are expected to be similar to those of the present study. For more general situations their flow characteristics and mixing behaviors require further investigations.

References

[1] A. Ajdari, Phys. Rev. Lett. 75 (1995) 755.
[2] A. Ajdari, Phys. Rev. 61 (2000) R45.
[3] A.D. Stroock, M. Weck, D.T. Chiu, W.T.S. Huck, P.J.A. Kenis, R.F. Ismagilov, G.M. Whitesides, Phys. Rev. Lett. 84 (2000) 3314.
[4] A.S. Panwar, S. Kumar, J. Chem. Phys. 118 (2003) 925.
[5] S. Qian, H.H. Bau, Anal. Chem. 74 (2002) 3616.
[6] H.J. Aref, J. Fluid Mech. 143 (1984) 1.
[7] J.M. Ottino, The Kinetics of Mixing: Stretching, Chaos, and Transport, Cambridge Univ. Press, New York, 1989.
[8] J.C. Baygents, T.L. Sounart, Colloids Surf. A 195 (2001) 59.
[9] J.L. Anderson, Annu. Rev. Fluid Mech. 21 (1989) 61.
[10] M.P. Hughes, R. Pethig, X.-B. Wang, J. Phys. D 29 (1996) 474.